Chapter 5
Controlling Morphology Using Low Molar Mass Nucleators

Geoffrey R. Mitchell, Supatra Wangsoub, Aurora Nogales, Fred J. Davis, and Robert H. Olley

5.1 Introduction

Crystallisation is a hugely important process in physical sciences and is crucial to many areas of, for example, chemistry, physics, biochemistry, metallurgy and geology. The process is typically associated with solidification, for example, in the purification of solids from a heated saturated solution familiar to all chemistry undergraduates. Crystalline solids are also often the end result of cooling liquids, or in some cases gases, but in order to form require nucleation, in the absence of nucleation supercooling of liquids well below the melting point is possible (Cavagna 2009). The quality of crystals, as gauged by size and levels of order, is highly variable, and will depend on factors such as material purity and the rate of cooling; rapid cooling may result in poor crystallisation, or even the formation of amorphous materials with no long-range order. In geological systems rates of cooling may vary over many orders of magnitude, for example, obsidian is a largely amorphous material produced when lava is rapidly cooled (Tuffen et al. 2013),

G.R. Mitchell (✉)
Centre for Rapid and Sustainable Product Development, Institute Polytechnic of Leiria, Marinha Grande, Portugal
e-mail: geoffrey.mitchell@ipleiria.pt

S. Wangsoub
Department of Chemistry, Naresuan University, Phitsanulok, Thailand

A. Nogales
Instituto de Estructura de la Materia, CSIC, Madrid, Spain

F.J. Davis
Department of Chemistry, The University of Reading, Whiteknights, Reading RG6 6AD, UK

R.H. Olley
Electron Microscopy Laboratory, The University of Reading, Whiteknights, Reading RG6 6AF, UK

G.R. Mitchell, A. Tojeira (eds.), *Controlling the Morphology of Polymers*,
DOI 10.1007/978-3-319-39322-3_5

Fig. 5.1 Giant gypsum crystals in the Cueva de los Cristales in Chihuahua, Mexico, the scale is indicated by the person (photo A. Van Driessche)

while the gypsum crystals found in the Cueva de los Cristales in Chihuahua, Mexico can reach 10 m in length (Fig. 5.1) and are formed over hundreds of thousands of years. In this latter case, the formation of such large spectacular structures as shown in Fig. 5.1 can only be explained by a low nucleation rate (García-Ruiz et al. 2007; Van Driessche et al. 2011).

Crystallisation from solution is a core technology in major areas of the chemical industry and it is the critical initial step in many scientific programmes including structural studies of proteins and pharmaceuticals. The process of nucleation by which embryonic crystals form within a supersaturated solution remains largely unexplained. In classical nucleation theory, the volume excess free energy of the nuclei at a critical radius balances the surface excess free energy; nuclei larger than this critical radius grow, and smaller entities dissolve back into the solution. Recently, other pathways of transformation have been identified theoretically in which structure and density fluctuations are separated (Kashchiev et al. 2005). In terms of controlling morphology in polymers, nucleation of polymer crystals plays an important part in the production of several commodity plastics, giving the potential for control of the polymer microstructure and therefore the subsequent properties (Bassett 2006). Nucleating agents are thus of considerable commercial and scientific interest. One well-known example of a nucleating agent is 1,3:2,4-dibenzyline sorbitol (I) (DBS) the structure of which is shown in I; this is extensively used as a clarification agent with polypropylene. Its use leads to transparent materials with improved mechanical properties (Zweifel 2001). This chapter focuses on the use of nucleating agents to control the structure and morphology of polymers and focuses particularly on DBS and its derivatives (Nogales and Mitchell 2005 Nogales et al 2003b; Nogales et al. 2016). In particular the work describes the self-assembly of such materials to form a template which can direct the crystallisation of polymers such as poly(ε-caprolactone) (Siripitayananon 2004).

I

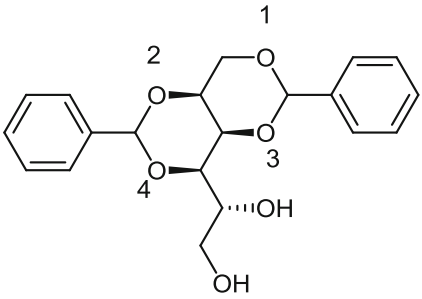

5.2 Organic Gelators

In general, gels are viscoelastic solid-like materials comprising an elastic cross-linked network and a solvent, which is the major component. The solid-like appearance of a gel is a result of the entrapment and adhesion of the liquid in the large surface area solid 3D matrix. DBS is an example of a low molar mass organic gelator (Terech and Weiss 1997) whose structure is shown in I; that is a gel derived from low molar mass compounds formed through self-aggregation of the small gelator molecules to produce entangled self-assembled fibrils (Smith 2009; Sangeetha and Maitra 2005). In the case of DBS typically these fibrils are of the order of about 10 nm in diameter and at sufficiently high DBS concentrations (generally less than 2 wt% depending on factors such as temperature and matrix polarity), the nanoscale fibrils form a three-dimensional network that promotes physical gelation in a wide variety of organic solvents and polymers.

The structures and properties of DBS-organogels formed in different solvents are well studied by Yamasaki and Tsutsumi (Yamasaki and Tsutsumi 1994, 1995; Yamasaki et al. 1995; Watase and Itagaki 1998). All of those studies show that DBS builds up helically twisted fibres in low viscosity solvents. This is accompanied by a tremendous change in the rheological properties of these materials, as self-assembly leads to gelation. This gelation is based on physical interaction between the molecules. Gelation depends on various factors, such as gelator concentration, temperature and solvent polarity. It has also been shown (Yamasaki and Tsutsumi 1995) that the DL-racemate is not able to self-aggregate; thus, chirality seems important in the self-organisation of DBS (though it might be expected that the L-enantiomorph would assemble in a similar form). Wangsoub et al. (2016a, b) have reported the properties and structure of gels formed from alkanes and dibenzylidene sorbitol, and the results are relevant in part to the use of DBS with polyethylene.

Gels of low molecular mass compounds are usually prepared by heating the gelator in an appropriate solvent and cooling the resulting isotropic supersaturated solution to room temperature. When the hot solution is cooled, the molecules start to condense and three situations are possible Fig. 5.2: (1) a highly ordered aggregation giving rise to crystals i.e. crystallisation, (2) a random aggregation resulting

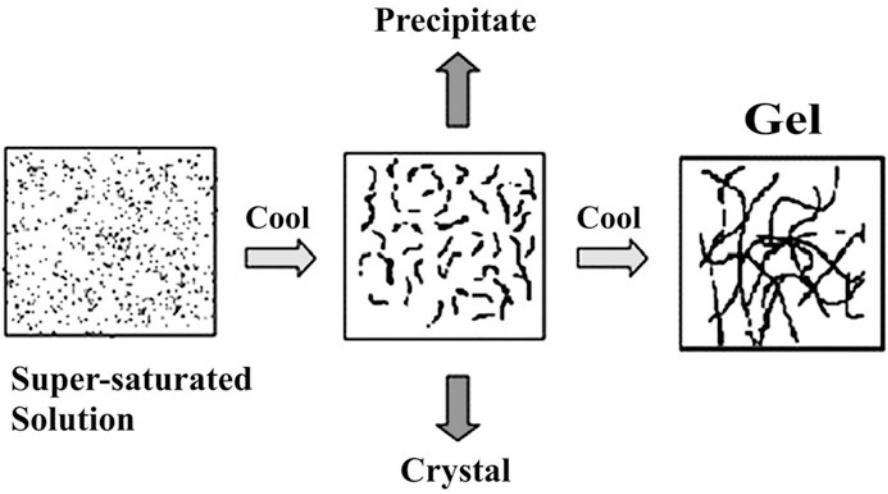

Fig. 5.2 Schematic representation of aggregation modes (redrawn after Sangeetha and Maitra 2005)

in an amorphous precipitate, and (3) and aggregation process intermediate between these two yielding a gel (1). The process of gelation involves self-association of the gelator molecules to form long, polymer-like fibrous aggregates, which get entangled during the aggregation process forming a matrix that traps the solvent mainly by surface tension. This process prevents the flow of solvent under gravity and the mass appears like a solid. At the microscopic level, the structures and morphologies of molecular gels have been investigated by conventional imaging techniques such as SEM, TEM and AFM. At the nanoscale, X-ray diffraction, small angle neutron scattering and X-ray scattering (SANS, SAXS) are required to elucidate the structures(Grubb et al 1975).

5.3 Synthesis of Sorbitol Derivatives

D-Sorbitol, or D-glucitol, is a sugar alcohol that is produced commercially by the reduction of glucose, but is also found naturally in many fruits. It finds many uses as an ingredient in the food industry and as such is designated E420 (Hanssen and Marsden 1984), though its use has been tainted with problems such as diarrhoea and flatulence. The dibenzylidene derivative is the main product of treatment with benzaldehyde, though mono and trisubstituted by-products may also be formed. Degradation and other studies confirmed that it is the 1,3:2,4 diacetal that is formed (Okesola et al. 2015). A range of other derivatives can be readily formed by the acid catalysed reaction of sorbitol with the appropriate substituted aldehyde (e.g. benzaldehyde, benzaldehyde d_6 or 4-chlorobenzaldehyde) in cyclohexane

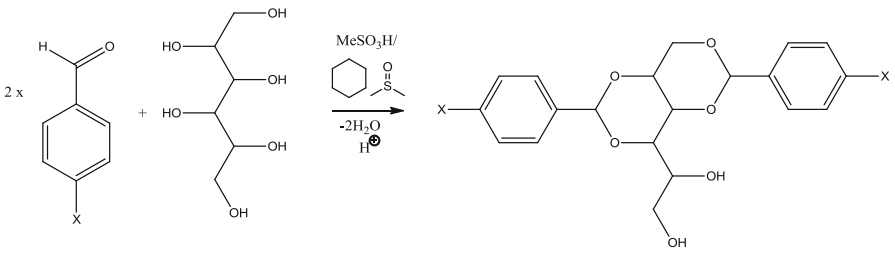

Scheme 5.1 Synthesis of Sorbitol derivatives

(Wangsoub et al. 2008). A typical procedure that for 1,3:2,4-di(4-chlorobenzylidene) sorbitol (Scheme 5.1) was as follows. An aqueous solution of D-sorbitol (0.1 mol, 70 % w/v) was placed into a round bottom flask equipped with Dean-Stark trap and condenser. To this was added 4-chlorobenzaldehyde (0.2 mol) and methanesulfonic acid (1 mL), cyclohexane (200 mL) and dimethylsulfoxide (6 mL). The mixture was heated to reflux with constant stirring. The mixture of cyclohexane and water was condensed and separated in the Dean-Stark arrangement. Once no further water was produced the reaction was stopped, and following neutralisation with triethylamine the white precipitate collected. Following purification by washing with dioxane and water 1,3:2,4-di(4-chlorobenzylidene) sorbitol was obtained as a white powder. The product was greater than 98 % pure by ^{1}H NMR,with a yield of 19.7 g, (46%) and a melting point of 187 °C.

5.4 DBS in Polymers

DBS and its derivatives can be easily dispersed in polymers using either melt mixing or mixing using a common solvent and drying. For the results shown here, the latter approach was used due to the small volume of material required. In this work we used the shear flow cell (Nogales et al. 2004) shown in Chap. 3 (Fig. 3.22) and for this, samples were prepared by co-solvent mixing, for example, with PCL we employed butanone, drying and then melt pressing into discs.

Figure 5.3 shows the phase behavior of the Cl-DBS/PCL system (Wangsoub et al. 2008). The line for the crystallisation temperature shows that the addition of the Cl-DBS increases the crystallisation temperature by ~10 °C due to the nucleating effect of the DBS derivative. This effect saturates at 1 % with Cl-DBS/PCL in contrast to ~3 % for DBS/PCL (Wangsoub et al. 2005). The upper curve shows the liquidus line separating the high temperature homogenous melt from the lower temperature 2-phase state of molten PCL and crystalline Cl-DBS fibrils. The liquidus line is shifted upwards by ~20 °C from the equivalent line for the DBS/PCL system (Wangsoub et al. 2005) indicating a reduced solubility for Cl-DBS in PCL.

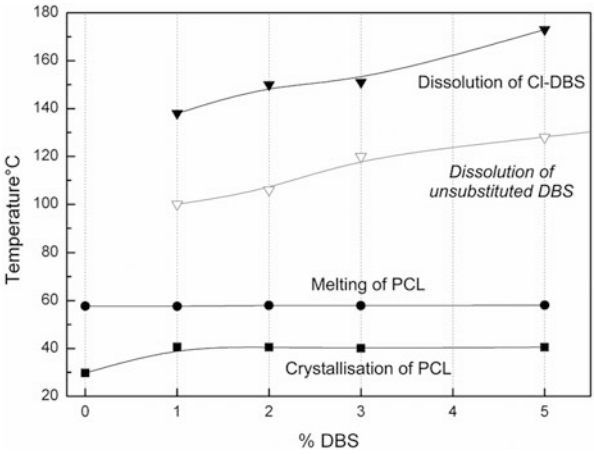

Fig. 5.3 A part of the phase diagram for the PCL, Cl-DBS system with the liquidus line for Cl-DBS/PCL (*inverted filled triangles*) and the liquidus line for DBS/PCL (*inverted open triangles*), PCL melting point (*filled circles*) and the PCL crystallisation temperature on cooling from the single phase melt (*filled squares*). Redrawn from Wangsoub et al. (2008)

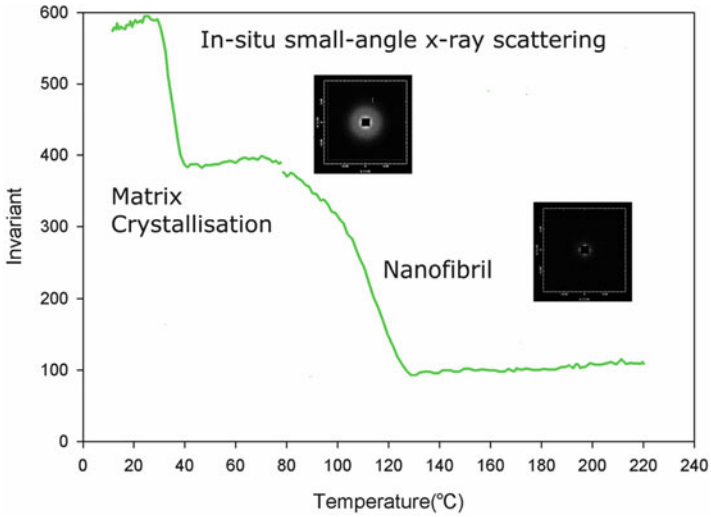

Fig. 5.4 A plot of the SAXS invariant Ω, (*5.1*) obtained from a sequence of time-resolving SAXS patterns recorded whilst cooling a 3 % Cl-DBS/PCL system from the higher temperature single phase region to room temperature at 10 °C/min (redrawn from Mitchell 2013). The *insets* show SAXS patterns taken at the temperatures corresponding to their position on the temperature scale

The phase behavior of the DBS or DBS derivative is dependent on both the chemical nature of the additive and the polarity of the polymer. For example, with DBS in PCL, the nucleating effect saturates at ~3 % whereas in polyethylene it saturates at a much lower concentration (Nogales et al. 2003a).

Figure 5.4 shows the results of a cooling experiment from the single homogenous phase of a composition of 3 % Cl-DBS in PCL in which we plot the invariant (5.1) calculated from the SAXS patterns recorded in a time-resolved manner. Each

SAXS pattern was recorded as a 2d dataset $I(\underline{Q}, \alpha)$. The invariant Ω was calculated using (5.1) (Mitchell 2013):

$$\Omega = \int_0^{\pi/2} \int_{Q=0}^{Q_{\max}} \left|\underline{Q}\right|^2 I\left(\left|\underline{Q}\right|, \alpha\right) \sin\alpha \, \mathrm{d}Q \, \mathrm{d}\alpha \tag{5.1}$$

The invariant is related to the average of the electron density differences and for example in the early stages of crystallisation, it is proportional to the volume of crystals. In (5.1), $\underline{Q}$ is the scattering vector, whose magnitude is given by $4\pi\sin(\theta)/\lambda$, where 2θ is the scattering angle and λ is the wavelength of the incident X-rays. α is the angle between a specific direction and the scattering vector.

Initially the invariant has a low value and falls slightly with reduced temperature. At $T \sim 127$ °C, the invariant increases sharply and this corresponds to formation of nanofibrils. Eventually at lower temperatures, the invariant plateaus and slightly falls. When the temperature reaches 40 °C, there is a second increase in the invariant which corresponds to the crystallisation of the PCL. It is clear that these two different ordering processes occur quite separately from each other. We can obtain more information about the state of the Cl-DBS in the 2-phase region by subjecting the material to a shear flow which leads to alignment of the Cl-DBS fibrils.

Figure 5.7a shows the SAXS pattern recorded in the 2-phase region. The horizontal streak corresponds to highly anisotropically shaped objects aligned parallel to the shear flow direction. Analysis of this scattering shows that it arises from objects with a radius of ~14 nm and a length greater than 100 nm (Wangsoub and Mitchell 2009). It is clear that a high level of anisotropy of these objects is achieved at modest shear rates. The level of anisotropy that can be achieved will also depend on the polymer and its molecular weight distribution.

Wangsoub et al. have reported the effects of the molecular weight distribution in the Polyethylene/DBS system (Wangsoub et al. 2016a, b). Samples were subjected to the same shear/temperature profile of 1000 shear units at 10 s^{-1} at temperatures considerably higher than the melting point of each material. After cooling to room temperature at 10 °C/min the samples were examined using wide-angle X-ray scattering and the azimuthal profiles for the 110 reflection are shown in Fig. 5.5. The lowest two molecular weight matrix polymers, PE190 and GA, show only a modest level of anisotropy as judged from the small variation in intensity with azimuthal angle, whereas the highest two molecular weight matrix polymers, GX and PE26, show a marked level of anisotropy. We attribute this to the stress which develops during shearing in the melt and its effect of the orientation of the DBS fibrils. In the curve for 1 %DBS/PE26, the high molecular weight matrix polymer, there is evidence for a range of lamellar tilt angles, in the form of a four point pattern which usually occurs when the matrix polymer is under stress in the typical shish kebab structures (Pople et al. 1999; Olley et al. 2014).

We have tested the effect of the DBS on the long period of the polyethylene GX and as Fig. 5.6 shows for samples crystallised at different temperatures the long

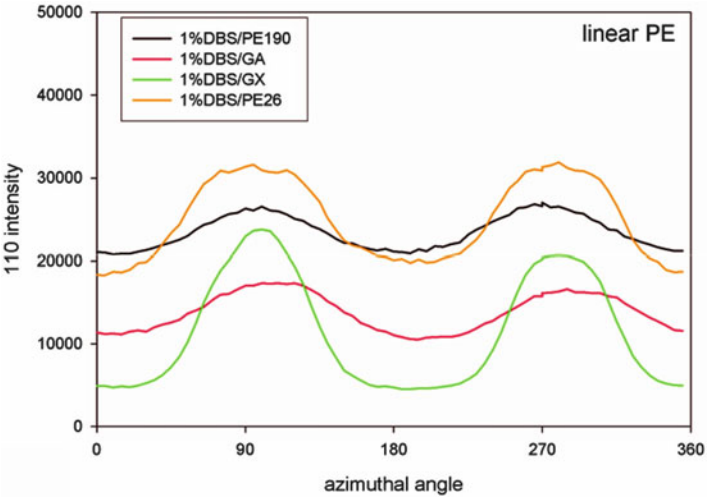

Fig. 5.5 WAXS Azimuthal profiles for the 110 reflection in Linear Polyethylene samples with different molecular weight distributions as listed in Table 5.1 containing 1 % DBS crystallised from a sheared melt as described in the text

Fig. 5.6 The long periods for a series of polyethylenes crystallised at differing temperatures for polyethylenes GX with and without DBS as indicated in the key

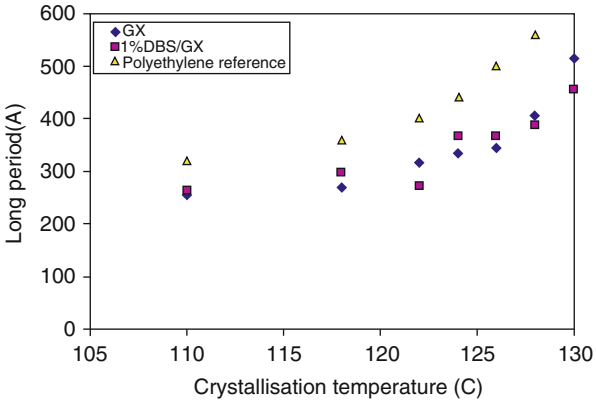

Table 5.1 Molecular weight characteristics of polymers used in the experiments reported in Fig. 5.5

Polymer	Mw	Mn	Mv	Type
Polymer code	Mw	Mn	Mv	Type
PE190	18,700	5410	10,000	Linear
GA	70,950	6250	45,000	Linear
GX	163,100	17,650	105,000	Linear
PE26	424,150	97,650	350,000	Linear

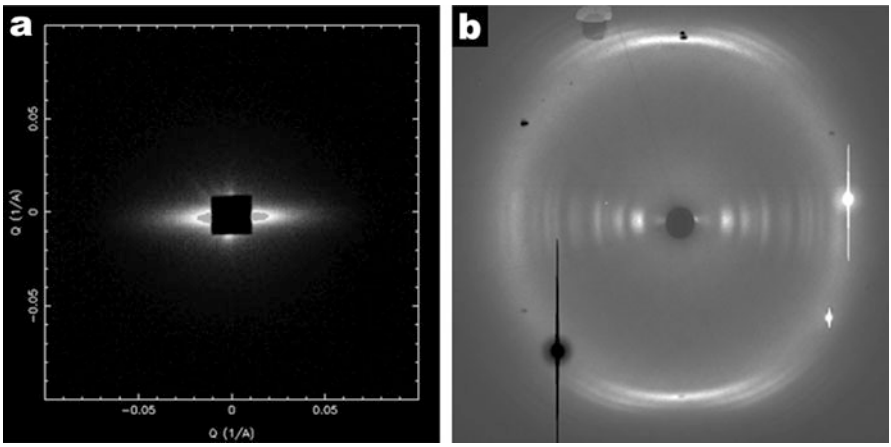

Fig. 5.7 (**a**) SAXS and (**b**) WAXS patterns recorded for a sample of Cl-DBS/PCL during shear flow 10 s^{-1} in the 2-phase region of the phase diagram

period for GX alone or GX/DBS is essentially the same. In other words the role of the DBS is to direct the crystallisation of the polymer, the lamellar structure remaining unaffected.

Figure 5.7b shows the WAXS pattern for the equivalent system to that shown in Fig. 5.7a. The figure is a difference between the pattern recorded in the 2-phase region and that recorded in the homogenous high temperature phase. As the scattering from the molten polymer and the crystallised DBS will be additive, we can subtract the polymer scattering to give a clearer view of the pattern of the additive.

It is clear that the Cl-DBS exhibits an ordered crystalline phase. It is interesting that the DBS fibrils are crystalline. This gives them different physical characteristics to other fibrillar gel systems such as self-assembling polypeptide gels and the worm-like micellar systems. The crystal structure leads to very rapid crystal growth in one direction, whereas in the lateral direction, the crystal growth is slower and more fragile. As discussed elsewhere this may be a consequence of the chiral nature of the structures. Optical microscopy studies have shown that the DBS nucleates crystallisation of the DBS from the single phase melt of polymer and DBS. Shear flow may lead to breakage of fibrils whereas the self-assembled micellar systems are virtual polymers and can pass through each other by breaking and reforming. There is good experimental evidence that shear flow leads to some breakage of fibrils. Of course reheating to the single phase region and subsequent crystallisation would lead to repair but loss of any anisotropy which had developed.

Prolonged shearing of the system shown in Fig. 5.7 leads to some unexpected changes. The sequence of SAXS patterns in Fig. 5.8 shows the effect increasing shear strain. We attribute the appearance of additional peaks in the pattern to a narrowing of the fibril diameter distribution. We have analysed the results using a Monte Carlo methodology to fit to Gaussian Distribution of Cylinder radii

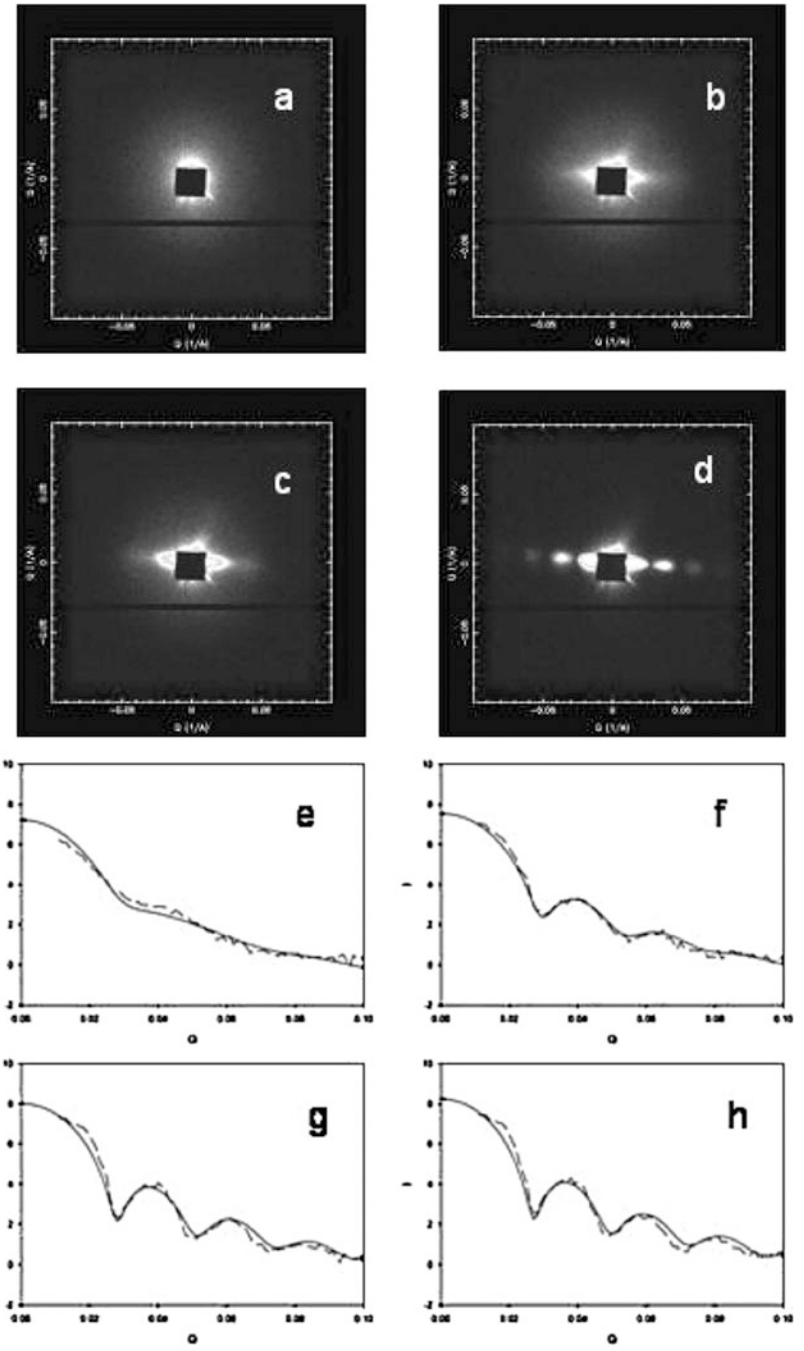

Fig. 5.8 Selected SAXS patterns corresponding to shear strains of (**a**) 0, (**b**) 100 su, (**c**) 10,000 su and (**d**) 28,000; (**e**–**h**) Equatorial sections (*broken lines*) corresponding to shear strains of (**e**) 1000 su (**f**) 4000 su, (**g**) 13,000 su and (**h**) 28,000 su taken from patterns from the same series as shown in (**a**–**d**) but for the shear strains indicated. The *full lines* in the sections correspond to the best-fit

(Wangsoub and Mitchell 2009). The extracted results are shown in Fig. 5.9 with plots of the mean radius which is largely unchanged and the Gaussian radius distribution b. The width reduces sharply and reaches a plateau value between 5000 and 10,000 shear units (shear rate × time of shearing).

Of other sugar alcohols, debenzylidene xylitol is widely used as a gelling agent; moreover, the three enantiomeric carbons in xylitol are arranged like a sequence of three carbons in xylitol. Dibenzylidene xylitol has been specified in the literature as a nucleating agent for polymers, but was not found to have any significant directing effect in polypropylene or polycaprolactone.

In contrast to the generation of row nuclei in polymers with a high molecular weight tail in the distribution, cessation of shear flow does not immediately lead to the relaxation of the oriented row nuclei. The aligned DBS fibrils remain aligned for quite some period (hours) which will doubtlessly in some cases lead to difficulty with experiments whilst attempting to remove prior history. Of course it may also prompt some novel methods of developing the anisotropy.

5.5 DBS Directing Crystallisation

We have shown in Sect. 5.4 how by using shear flow in conjunction with a polymer containing a DBS derivative we can obtain aligned nanoscale fibrils which are arranged parallel to the shear flow. This can be achieved while the matrix polymer is in the molten state. If we now crystallise the sample, we can exploit these extended objects as row nuclei to direct the crystalline morphology of the matrix polymer. Figure 5.10 shows a SAXS pattern recorded at Diamond on beamline I22 using the shear flow cell with Cl-DBS/PCL sample, after a cycle of shearing and cooling. The horizontal streak around the beam stop corresponds to the highly extended fibrils about 14–15 nm radius and greater than 100 nm long. The features above and below the beam stop are typical of small-angle scattering from semi-crystalline polymers and relate to the lamellar crystal morphology. Clearly the level of preferred orientation of both the nanofibrils and the crystal lamellae is very high.

Figure 5.11 shows the same type of information but revealed using electron microscopy coupled with differential etching. The extended object in the centre of the image is the impression of the DBS fibrils left in the polymer matrix after it was removed by etching. We can see that the main object is made up of smaller fibrils fused together. The highly aligned lamellae, seen here edge on, are easily visible and their geometric arrangement to the DBS nanofibrils is clear. In the following two images, the directing influence of the DBS nanofibrils can be easily observed. In Fig. 5.9b to the left beyond the end of the impression left by the nanofibril we can

Fig. 5.8 (continued) model for a set of polydisperse cylinders. The fitting parameters are plotted in Fig. 5.9. The horizontal black bar in the lower half of each pattern arises from a defect in the detector system during the measurements

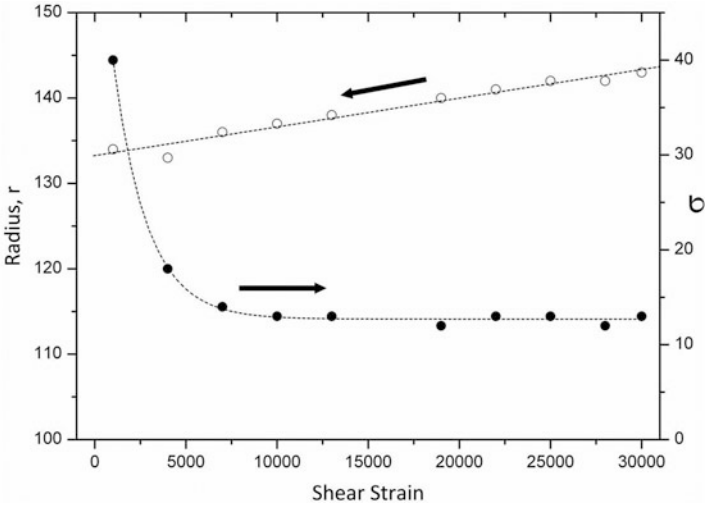

Fig. 5.9 Plots of the mean diameter and the standard deviation of the Gaussian radius distribution as a function of increasing shear strain obtained from SAXS data using a Monte Carlo approach (redrawn from Wangsoub and Mitchell (2009))

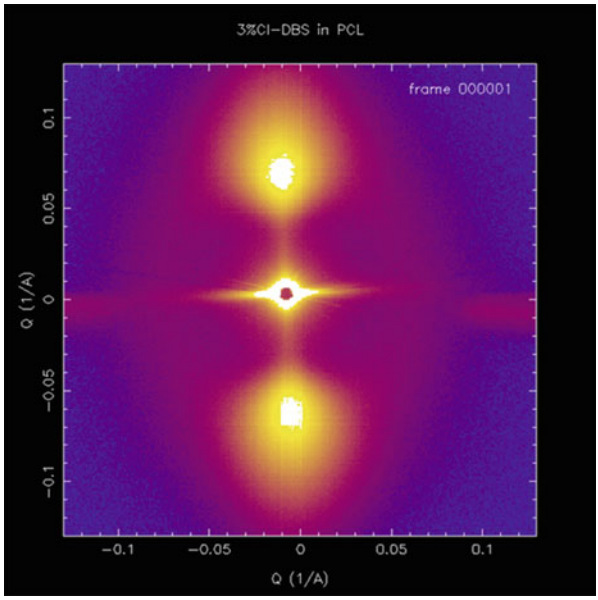

Fig. 5.10 Shows the SAXS pattern recorded for the 3 % Cl-DBS/PCL system after shearing at 80 °C at a shear rate of 10 s^{-1} This pattern was obtained at the Diamond Light Source beam line I22 (redrawn from Mitchell 2013)

see a more random arrangement of lamellae. In fact we can now see some face on. Furthermore between the two nanofibrils which are not quite parallel with each other we can the two sets of directed lamellae impacting in the centre portion (Fig. 5.12).

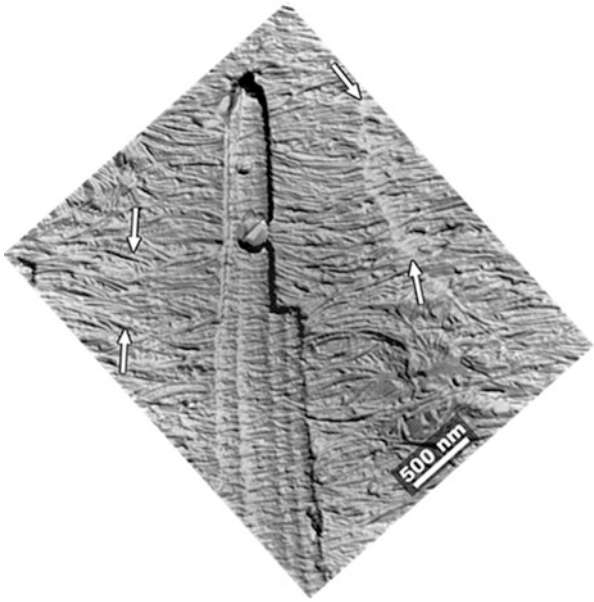

Fig. 5.11 Transmission electron micrograph of a replica of a differentially etched interior surface of polyethylene sample containing DBS

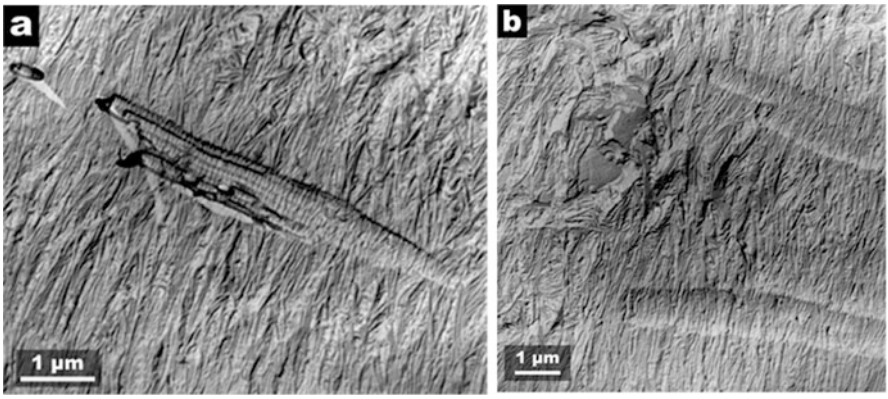

Fig. 5.12 (**a**) Detail of a single cluster of DBS fibres (**b**) Polyethylene development from DBS fibres, *right*, compared with general development, *left*

Figure 5.13 shows the interior surface of DBS/PE system (Wangsoub et al 2016b) prepared by cutting a sheared disc in half. We are now looking in a direction parallel to the aligned nanofibrils. The holes correspond to where the nanofibrils were, and subsequent etching has broadened the hole from its original size. We can see the excellent dispersion of the DBS nanofibrils.

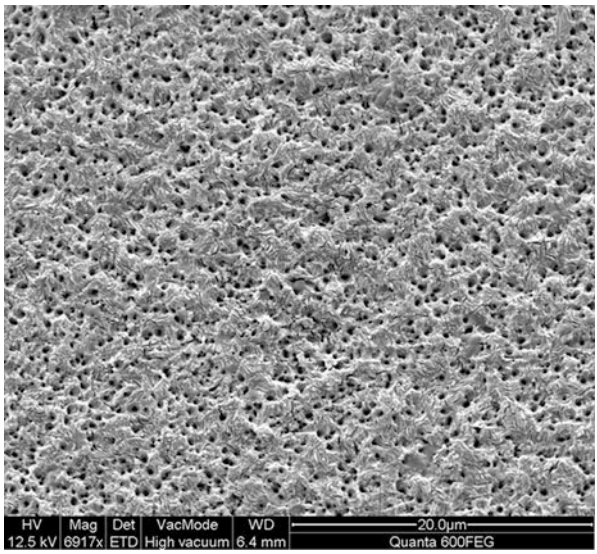

Fig. 5.13 A scanning electron micrograph of the surface of section cut through a sheared disc which was crystallised from a sheared melt of PE/DBS. The surface is perpendicular to the alignment of the DBS fibrils

5.6 Model of Directed Crystallisation

In the case of highly aligned fibrils, consideration of the templating process reduces to a 2-d matter. The number density of fibrils is given by Wangsoub et al. (2008)

$$N = {}^{(f-f_c)}/_{\pi r_f^2}$$

where f is the fraction of the additive and f_c is the upper limit of solubility of the additive in the polymer matrix. We consider all fibrils to have the same radius r_f.

If we associate a templated zone of radius r_t with each fibril, the fraction of templated material, f_t, (Fig. 5.14) is given by:

$$f_t = (f - f_c)\frac{\pi r_t^2}{\pi r_f^2}$$

Clearly, this is a very simple model without any distribution of fibril dimensions and the templated zone size does not account for a random spatial distribution of fibrils. However, we do have an estimate of the fibril radius of ~7.5 nm from the SAXS measurements and we have estimated for polyethylene that the templated zone has a radius ~100 nm. This suggests that the value of $(f-f_c)$ needs to be greater than 0.014 to achieve full templating. Clearly the solubility of the sorbitol derivative in the polymer matrix is critical in determining the actual amount of additive required to achieve this. We previously estimated that the solubility limit of DBS in PCL was ~0.01 and we attribute in large part the enhanced templating of Cl-DBS to a reduction in the solubility limit in PCL. This is shown in the DSC and

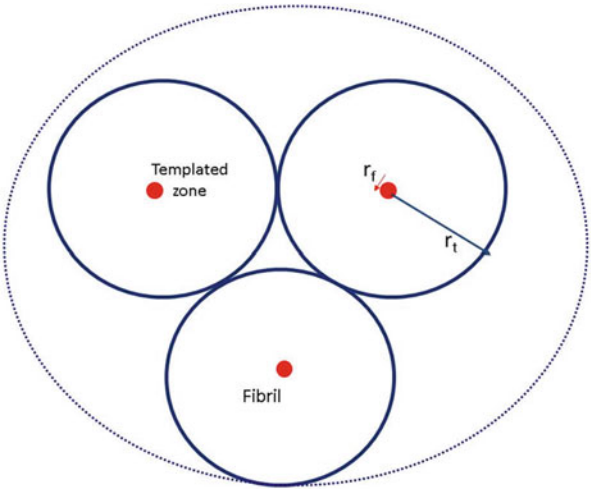

Fig. 5.14 Schematic of model to examine the templating process with nanoscale fibrils of DBS in a polymer. This is section taken normal to the fibril axis

liquidus line. In the examples of the morphology shown in Figs. 5.8, 5.9 and 5.10, the directing is more or less perfect and the hence the orientation parameter $\langle P_2 \rangle_L$ describing the preferred orientation of the lamellae with respect to the flow axis is given by the fraction of material templated:

$$\langle P_2 \rangle_L = -0.5(f - f_c)\frac{\pi r_t^2}{\pi r_f^2}$$

The factor −0.5 (Lovell and Mitchell 1981) takes account of the fact that the lamellae are arranged normal to the flow axis. The efficacy of the templating or directing process depends on the number density of the DBS fibrils. For a given amount of DBS, the number density can be optimised by making the nanofibrils as thin as possible. The processes described in this chapter are effective because of the lateral nanoscale of the fibrils.

5.7 Summary

We have shown that the inclusion of small amounts of DBS or selected derivatives leads to the formation of a well-dispersed system of nanofibrils. These are particularly effective in directing the crystallisation of polyethylene, polypropylene and poly(ε-caprolactone) due to the high number density of the fibrils in the sample. It may well be possible to extend to other polymer systems. Such work is underway. The approach offers distinct advantages over the other approaches described in other chapters in this volume. It avoids the use of viscous high molecular fractions to produce row nuclei. By using a nanoparticle it may be possible to achieve other

orientations of the nanoparticles than parallel to the flow axis. The latter takes place because of the high level of anisotropy of the nanofibrils. The high aspect ratio of the nanofibrils means that any deformation of the polymer melt is likely to lead to a high level of orientation of the nanofibrils leading to a high level of preferred orientation of the lamellar crystals.

Acknowledgements This work was supported by the Fundação para a Ciência e a Tecnologia (Portugal) through project PTDC/CTM-POL/7133/2014 and through the Project reference UID/Multi/04044/2013.

We thank Naresuan University for supporting SW during her Ph.D. programme and the Faculty of Science at Naresuan University for funding subsequent short visits when much of the work described here was performed.

This chapter contains various data recorded at international synchrotron and neutron scattering facilities. We are indebted to those facilities for access and to the beamline scientists for their involvement in these experiments; Dr. Sigrid Bernstoff (Elettra), Dr. Francois Fauth (ESRF), Dr. Sergio Funari (Hasylab), Dr. Jen Hiller and Dr. Nick Terrill (Diamond), Dr. Steve King, Dr. Sarah Rogers, Dr. Ann Terry and Dr. Richard Heenan (ISIS).

References

Bassett DC (2006) Linear nucleation of polymers. Polymer 47:5221–5227

Cavagna A (2009) Supercooled liquids for pedestrians. Phys Rep 476(4–6):51–124

García-Ruiz JM, Villasuso R, Ayora C, Canals A, Otálora F (2007) Formation of natural gypsum megacrystals in Naica, Mexico. Geology 35(4):327–330

Grubb DT, Dlugosz J, Keller A (1975) Direct observation of lamellar morphology in polyethylene. J Mater Sci 10:1826–1828

Hanssen M, Marsden J (1984) E for additives: the complete E number guide. Thorsons, Wellingborough

Kashchiev D, Vekilov PG, Kolomeisky AB (2005) Kinetics of two-step nucleation of crystals. J Chem Phys 122:244706

Lovell R, Mitchell GR (1981) Molecular orientation distribution derived from an arbitrary reflection. Acta Cryst A37:135–137

Mitchell GR (2013) Characterisation of safe nanostructured polymers. In: Silvestre C, Cimmino S (eds) Ecosustainable polymer nanomaterials for food packaging. Taylor and Francis, Boca Raton, Print ISBN: 978-90-04-20737-0, eBook ISBN: 978-90-04-20738-7

Nogales A, Mitchell GR (2005) Development of highly oriented polymer crystals from row assemblies. Polymer 46:5615–5620

Nogales A, Olley RH, Mitchell GR (2003a) Directed crystallisation of synthetic polymers by low-molar-mass self-assembled templates. Macromol Rapid Commun 24:496–502

Nogales A, Mitchell GR, Vaughan AS (2003b) Anisotropic crystallization in polypropylene induced by deformation of a nucleating agent network. Macromolecules 36:4898–4906

Nogales A, Thornley SA, Mitchell GR (2004) Shear cell for in-situ WAXS, SAXS and SANS experiments on polymer melts under flow fields. J Macromol Sci Phys B43:1161–1170

Nogales A, Olley RH, Mitchell GR (2016) On morphology of row structures in polyethylene generated by shear alignment of dibenzylidene sorbitol. J Polym Res (Submitted)

Okesola BO, Vieira VMP, Cornwell DJ, Whitelaw NK, Smith DK (2015) 1,3:2,4-Dibenzylidene-D-sorbitol (DBS) and its derivatives—efficient, versatile and industrially relevant low-molecular-weight gelators with over 100 years of history and a bright future. Soft Matter 11:4768–4787

Olley RH, Mitchell GR, Moghaddam Y (2014) On row-structures in sheared polypropylene and a propylene-ethylene copolymer. Eur Polym J 53:37–49

Pople JA, Mitchell GR, Sutton SJ, Vaughan AS, Chai C (1999) The development of organised structures in polyethylene crystallised from a sheared melt, analyzed by WAXS and TEM. Polymer 40:2769–2777

Sangeetha NM, Maitra U (2005) Supramolecular gels: functions and uses. Chem Soc Rev 34:821–836

Siripitayananon J, Wangsoub S, Olley RH, Mitchell GR (2004) The use of a low-molar-mass self-assembled template to direct the crystallisation of poly (epsilon-caprolactone). Macromol Rapid Commun 25:1365–1370

Smith DK (2009) Lost in translation? Chirality effects in the self-assembly of nanostructured gel-phase materials. Chem Soc Rev 38:684–694

Terech P, Weiss RG (1997) Low molecular mass gelators of organic liquids and the properties of their gels. Chem Rev 97(8):3133–3160

Tuffen H, James M, Castro J, Schipper CI (2013) Exceptional mobility of an advancing rhyolitic obsidian flow at Cordon Caulle volcano in Chile: observations from Cordón Caulle, Chile, 2011-2013. Nat Commun 4:2709. doi:10.1038/ncomms3709

Van Driessche AES, García-Ruíz JM, Tsukamoto K, Patiño-Lopez LD, Satoh H (2011) Ultraslow growth rates of giant gypsum crystals. Proc Natl Acad Sci U S A 108:15721–15726

Wangsoub S, Mitchell GR (2009) Shear controlled crystal size definition in a low molar mass compound using a polymeric solvent. Soft Matter 5:525

Wangsoub S, Olley RH, Mitchell GR (2005) Directed crystallisation of poly(ε-caprolactone) using a low-molar-mass self-assembled template. Macromol Chem Phys 206:1826–1839

Wangsoub S, Davis FJ, Mitchell GR, Olley RH (2008) Enhanced templating in the crystallisation of poly(ε-caprolactone) using 1,3:2,4-di(4-chlorobenzylidene) sorbitol. Macromol Rapid Commun 2008(29):1861–1865

Wangsoub S, Davis FJ, Harris PJF, Mitchell GR, Olley RH (2016a) Structure and morphology of high liquid content gels formed from alkanes and dibenzylidene sorbitol. Phys Chem Chem Phys (Submitted)

Wangsoub S, Olley RH, Mitchell GR (2016b) Templating the crystallisation of polyethylene using dibenzylidene sorbitol. Macromol Chem Phys (Submitted)

Watase M, Itagaki H (1998) Thermal and rheological properties of physical gels formed from benzylidene-D-sorbitol derivatives. Bull Chem Soc Jpn 71(6):1457–1466

Yamasaki S, Tsutsumi H (1994) Microscopic studies of 1,3: 2,4-di-O-benzylidene-D-sorbitol in ethylene glycol. Bull Chem Soc Jpn 67:906–911

Yamasaki S, Tsutsumi H (1995) The dependence of the polarity of solvents on 1,3: 2,4-di-*o*-benzylidene-D-sorbitol gel. Bull Chem Soc Jpn 68:123–127

Yamasaki S, Ohashi Y, Tsutsumi H, Tsujii K (1995) The aggregated higher-structure of 1,3: 2,4-di-*o*-benzylidene-D-sorbitol in organic gels. Bull Chem Soc Jpn 68:146–151

Zweifel H (2001) Plastics additives handbook. Hanser, Munich, Chapter 18